# A Graphical Approach to E-sail Mission Design with Radial Thrust

Giovanni Mengali,* Alessandro A. Quarta, Generoso Aliasi

*Dipartimento di Ingegneria Aerospaziale, University of Pisa, I-56122 Pisa, Italy*

**Abstract**

This paper describes a semi-analytical approach to electric sail mission analysis under the assumption that the spacecraft experiences a purely radial, outward, propulsive acceleration. The problem is tackled by means of the potential well concept, a very effective idea that was originally introduced by Prussing and Coverstone in 1998. Unlike a classical procedure that requires the numerical integration of the equations of motion, the proposed method provides an estimate of the main spacecraft trajectory parameters, as its maximum and minimum attainable distance from the Sun, with the simple use of analytical relationships and elementary graphs. A number of mission scenarios clearly show the effectiveness of the proposed approach. In particular, when the spacecraft parking orbit is either circular or elliptic it is possible to find the optimal performances required to reach an escape condition or a given distance from the Sun. Another example is given by the optimal strategy required to reach a heliocentric Keplerian orbit of prescribed orbital period. Finally the graphical approach is applied to the preliminary design of a nodal mission toward a Near Earth Asteroid.

*Key words:* Electric sail, Radial thrust, Potential well

* Corresponding author.
*Email addresses:* g.mengali@ing.unipi.it (Giovanni Mengali,), a.quarta@ing.unipi.it (Alessandro A. Quarta,), g.aliasi@dia.unipi.it (Generoso Aliasi).

## Nomenclature

$a$ = semimajor axis

$a_\oplus$ = E-sail characteristic acceleration

$\mathcal{E}$ = specific mechanical energy of the osculating orbit

$\mathcal{E}_w$ = potential well boundary

$e$ = eccentricity

$P$ = point in the energy plane

$p$ = semilatus rectum

$q$ = resonance ratio

$R$ = prescribed distance

$r$ = Sun-spacecraft distance ($r_\oplus \triangleq 1\,\mathrm{AU}$)

$T$ = orbital period

$t$ = time

$u$ = radial component of velocity

$V_\infty$ = hyperbolic excess velocity

$v$ = circumferential component of velocity

$\beta$ = dimensionless characteristic acceleration

$\theta$ = polar angle

$\mu_\odot$ = Sun's gravitational parameter

$\omega$ = argument of periapsis

*Subscripts*

$0$ = initial, parking orbit

$a$ = aphelion

$b$ = point on the potential well boundary

$e$ = escape

$j$ = jettison

$k$ = Keplerian

min = minimum

$n$ = Near Earth Asteroid

$p$ = perihelion

$t$ = tangent

☊ = ascending node

☋ = descending node

*Superscripts*

$\cdot$ = time derivative

$\sim$ = dimensionless value

$\star$ = critical value

## 1 Introduction

Due to their long flight times, space missions with low-thrust propulsion systems are usually studied in an optimal framework, by maximizing (or minimizing) a suitable scalar performance index. The latter coincides, for example, with the propellant mass for electrical propulsion systems [1,2] or with the total flight time for a propellantless thruster as a solar sail [3,4] or an electric sail [5,6,7,8,9,10]. The solution of the optimal control problem associated to the design of the space trajectory is the output of a complex numerical optimization process, and the solution is typically found using a dedicated software. Only in a few cases the optimal control problem can be fully solved in an analytical or graphical form. One of such special cases is represented by the problem of calculating the optimal escape conditions for a space vehicle with constant, outward, propulsive acceleration. The first solution to this problem was analytically found by Tsien [11] assuming that the spacecraft is placed on a parking circular orbit and, recently, was extended by Mengali and Quarta [12] to elliptical orbits using the potential well, a concept originally introduced by Prussing and Coverstone [13].

The aim of this paper is to introduce a graphical approach for the preliminary deep space mission analysis of an electric sail (E-sail) [7,14,15], whose attitude is oriented in such a way to provide a purely radial thrust along the whole heliocentric trajectory. The space vehicle is therefore subjected to a propulsive outward acceleration that, according to the most recent studies [16], varies inversely proportional to the Sun-spacecraft distance $r$. Following Prussing and Coverstone [13], when the propulsion system is switched on, the spacecraft trajectory can be mapped into an "energy plane", that is, the plane in which the specific mechanical energy of the osculating orbit is expressed as a function of the spacecraft radial distance from the primary. In particular, Prussing and Coverstone [13] suggest to partition the energy plane into allowed and forbidden regions using the so called potential well, which bounds the radial distance interval within which the spacecraft motion is feasible.

With the aid of a suitable choice of the independent variables, another definition of the energy plane, slightly different than that of Ref. [13], is now introduced. In this new energy plane, the specific mechanical energy of an E-sail depends linearly on the distance from the Sun, and its slope is proportional to the E-sail characteristic acceleration, that is, the maximum propulsive acceleration at a Sun-spacecraft distance equal to 1 Astronomical Unit (AU). The main results of a preliminary mission analysis are thus obtained by simply intersecting the potential well boundary with the line corresponding to the specific mechanical energy level.

## 2 E-sail Motion with Radial Thrust

Consider a spacecraft, of constant mass, that initially tracks a heliocentric closed parking orbit of semilatus rectum $p_0$ and eccentricity $e_0$. The spacecraft primary propulsion system is constituted by an E-sail with characteristic acceleration $a_\oplus$, which, by assumption, provides a radial outward thrust whose modulus is inversely proportional [16] to the Sun-spacecraft distance $r$.

The E-sail thrust is switched-on at $t = t_0 \triangleq 0$, and the succeeding spacecraft motion takes place in the plane of the parking orbit. The corresponding spacecraft equations of motion in a polar, heliocentric reference frame are [11,16]:

$$\dot{r} = u \tag{1}$$

$$\dot{\theta} = \frac{\sqrt{\mu_\odot \, p_0}}{r^2} \tag{2}$$

$$\dot{u} = \frac{\mu_\odot}{r^2}\left(\frac{p_0}{r} - 1\right) + a_\oplus \, \frac{r_\oplus}{r} \tag{3}$$

where $\theta$ is the polar angle measured counterclockwise from the direction of the parking orbit's eccentricity vector, $u$ is the radial component of the spacecraft velocity, $\mu_\odot$ is the Sun's gravitational parameter, and $r_\oplus \triangleq 1\,\text{AU}$ is a reference distance. In the special case of circular parking orbit ($e_0 = 0$), the polar angle $\theta$ is measured counterclockwise from the Sun-spacecraft direction at time $t_0$.

When Eq. (1) is substituted into (3), the following second order, nonlinear differential equation in the variable $r$ is obtained:

$$\ddot{r} = \frac{\mu_\odot}{r^2}\left(\frac{p_0}{r} + \beta \, \frac{r}{r_\oplus} - 1\right) \tag{4}$$

where the dimensionless characteristic acceleration $\beta$ is defined as

$$\beta = \frac{a_\oplus}{\mu_\odot / r_\oplus^2} \tag{5}$$

Note that $\beta$ plays the same role in the E-sail performance characterization as the lightness number [17] does for solar (or photonic) sails, when an ideal force model [18] is assumed. The boundary conditions of Eq. (4) are given by the Sun-spacecraft distance and the spacecraft radial component of velocity at the initial time $t_0$, that is:

$$r_0 = \frac{p_0}{1 + e_0 \cos\theta_0} \qquad , \qquad u_0 = \sqrt{\frac{\mu_\odot}{p_0}}\, e_0 \sin\theta_0 \tag{6}$$

where $\theta_0 \triangleq \theta(t_0)$ is the starting polar angle.

Taking into account the initial conditions (6), the first integral of the autonomous differential equation (4) is:

$$\frac{u^2 - u_0^2}{2} + \frac{\mu_\odot\, p_0}{2}\left(\frac{1}{r^2} - \frac{1}{r_0^2}\right) - \mu_\odot\left(\frac{1}{r} - \frac{1}{r_0}\right) - \beta\,\frac{\mu_\odot}{r_\oplus}\log\left(\frac{r}{r_0}\right) = 0 \tag{7}$$

Introduce now the specific mechanical energy $\mathcal{E}$ of the spacecraft heliocentric osculating orbit

$$\mathcal{E} = \frac{u^2}{2} + \frac{\mu_\odot\, p_0}{2\, r^2} - \frac{\mu_\odot}{r} \tag{8}$$

and observe that Eq. (7) can be written in a compact form as

$$\mathcal{E} = \mathcal{E}_0 + \beta\,\frac{\mu_\odot}{r_\oplus}\log\left(\frac{r}{r_0}\right) \tag{9}$$

where

$$\mathcal{E}_0 \triangleq \mathcal{E}(t_0) = \frac{u_0^2}{2} + \frac{\mu_\odot\, p_0}{2\, r_0^2} - \frac{\mu_\odot}{r_0} \tag{10}$$

is the specific mechanical energy of the spacecraft parking orbit. Note that the last term in Eq. (9) coincides with the work, per unit of mass, of the E-sail propulsive thrust corresponding to the radial displacement $\Delta r = r - r_0$.

According to Prussing and Coverstone [13], Eq. (9) maps the spacecraft motion into the "energy plane", that is, the plane where the osculating orbit's specific mechanical energy $\mathcal{E}$ is expressed as a function of the radial distance $r$. In this plane the spacecraft motion is from below constrained by the so called potential well [13], that is

$$\mathcal{E} \geq \mathcal{E}_w \tag{11}$$

where $\mathcal{E}_w$ is the minimum allowable value of the specific mechanical energy (corresponding to a given radial distance $r$) that is obtained from Eq. (8) by enforcing the condition [19] $u^2 \geq 0$, viz.

$$\mathcal{E}_w = \frac{\mu_\odot\, p_0}{2\, r^2} - \frac{\mu_\odot}{r} \tag{12}$$

The spacecraft heliocentric motion is better described using a modified energy plane $(\widetilde{\mathcal{E}}, \widetilde{r})$, which results from the introduction of the following dimensionless terms

$$\widetilde{\mathcal{E}} \triangleq \frac{\mathcal{E}}{\mu_\odot/r_0} \quad , \quad \widetilde{\mathcal{E}}_w \triangleq \frac{\mathcal{E}_w}{\mu_\odot/r_0} \quad , \quad \widetilde{r} \triangleq \log\left(\frac{r}{r_0}\right) \tag{13}$$

Bearing in mind Eq. (6), the expressions for $\widetilde{\mathcal{E}}$ and $\widetilde{\mathcal{E}}_w$ are:

$$\widetilde{\mathcal{E}} = \frac{e_0^2 - 1}{2\,(1 + e_0\,\cos\theta_0)} + \beta\,\frac{p_0}{r_\oplus\,(1 + e_0\,\cos\theta_0)}\,\widetilde{r} \tag{14}$$

$$\widetilde{\mathcal{E}}_w = \frac{(1 + e_0\,\cos\theta_0)}{2}\,\exp(-2\,\widetilde{r}) - \exp(-\widetilde{r}) \tag{15}$$

and Eq. (11) becomes:

$$\widetilde{\mathcal{E}} \geq \widetilde{\mathcal{E}}_w \tag{16}$$

From Eq. (15) it is clear that the shape of the potential well boundary $\widetilde{\mathcal{E}}_w = \widetilde{\mathcal{E}}_w(\widetilde{r})$ depends both on the parking orbit characteristics (through $e_0$) and on the initial spacecraft position $\theta_0$, but it is independent of the E-sail performance (quantified through the parameter $\beta$). On the contrary, for a circular parking orbit ($e_0 = 0$) the function $\widetilde{\mathcal{E}}_w$ is independent of $\theta_0$.

Moreover, Eq. (14) states that the dimensionless specific mechanical energy is a linear function of $\widetilde{r}$, and its slope is proportional to the dimensionless characteristic acceleration $\beta$. For a circular parking orbit ($\widetilde{r} = 0$), the initial value of the dimensionless specific mechanical energy is simply $\widetilde{\mathcal{E}} = -1/2$.

A graphical interpretation of Eqs. (14)-(15) provides valuable insights into the spacecraft heliocentric trajectory without the need of integrating the equations of motion (1)–(3). This matter is now illustrated in detail with the aid of a number of mission applications.

## 3 Minimum Propulsive Acceleration to Escape

As a first application of the previous concepts to an E-sail mission analysis, consider the problem of finding the minimum propulsive acceleration required to escape from the Sun when the propulsion system is operating for the whole mission duration. This is a classical problem that has been extensively studied in the literature, especially under the assumption of constant propulsive, outward, acceleration [11,13,19]. Here the minimum value of $a_\oplus$ [equivalently, the minimum $\beta$, see Eq. (5)] will be found graphically in the energy plane. The two cases of circular or elliptic parking orbit will be discussed separately.

### *3.1 Circular Parking Orbit*

The shape of the potential well $\widetilde{\mathcal{E}}_w = \widetilde{\mathcal{E}}_w(\widetilde{r})$ for a circular parking orbit of radius $r_0 \equiv p_0$ is shown in Fig. 1. Recall that the points below the potential well boundary belong to a forbidden region (shaded area in Fig. 1) where the spacecraft motion cannot take place.

According to Eq. (14), at the initial time $t_0$ the spacecraft position in the energy plane is represented by the point $P_0 = (0, -1/2)$, and the spacecraft radial velocity component at $t_0$ is zero. When the propulsion system is switched-on ($t > t_0$), the spacecraft at first increases both its specific energy $\widetilde{\mathcal{E}}$ and its distance from the Sun $\widetilde{r}$ moving along the straight line defined by Eq. (14). This line will be referred to as "energy line", and its slope is proportional to the dimensionless characteristic acceleration $\beta$. The spacecraft motion corresponds to one of the following three cases.

### 3.1.1 *Case a*

The energy line, with a slope $\beta^\star r_0/r_\oplus$, is tangent to the potential well boundary at point $P_t = (\tilde{r}_t, \tilde{\mathcal{E}}_t)$, see Fig. 1. In this case, the pair $(\tilde{r}_t, \beta^\star)$ is solution of the system of algebraic equations:

$$\tilde{\mathcal{E}} = \tilde{\mathcal{E}}_w \qquad \cap \qquad \frac{\partial \tilde{\mathcal{E}}}{\partial \tilde{r}} = \frac{\partial \tilde{\mathcal{E}}_w}{\partial \tilde{r}} \tag{17}$$

or, with the aid of Eqs. (14)–(15)

$$2\,\tilde{r}_t \exp\left(-\tilde{r}_t\right) \left[1 - \exp\left(-\tilde{r}_t\right)\right] - 1 = \exp\left(-\tilde{r}_t\right) \left[\exp\left(-\tilde{r}_t\right) - 2\right] \tag{18}$$

$$\beta^\star = \left(\frac{r_\oplus}{r_0}\right) \exp\left(-\tilde{r}_t\right) \left[1 - \exp\left(-\tilde{r}_t\right)\right] \tag{19}$$

whose solution is

$$\tilde{r}_t \simeq 1.256431 \qquad , \qquad \beta^\star \simeq 0.203632 \left(\frac{r_\oplus}{r_0}\right) \tag{20}$$

Substituting $\tilde{r}_t$ from (20) into Eq. (14), the energy at $P_t$ is $\tilde{\mathcal{E}}_t \simeq -0.244150$.

The spacecraft motion can now be qualitatively described as follows. When the propulsion system (whose dimensionless characteristic acceleration is $\beta^\star$, see Eq. (20)) is switched-on, the Sun-spacecraft distance increases following the segment $\overline{P_0 P_t}$. At time $t_t$ the spacecraft reaches the point $P_t$ whose distance from the Sun is

$$r_t \triangleq r_0 \exp(\tilde{r}_t) \simeq 3.512862\, r_0 \tag{21}$$

Here the spacecraft radial velocity component is zero, because $P_t$ belongs to the potential well boundary, while its radial acceleration component $\ddot{r}_t \triangleq \ddot{r}(r_t)$ is obtained from Eq. (4) with the substitution $\beta = \beta^\star$ and $r = r_t$. It can be verified that $\ddot{r}_t = 0$. Therefore, the spacecraft reaches $P_t$ with zero velocity and zero acceleration in the radial direction. Accordingly, for $t \geq t_t$ the spacecraft tracks a circular, non-Keplerian [6,20], orbit of radius $r_t$ with a constant velocity $v = \sqrt{\mu_\odot\, p_0}/r_t$, as is shown in Fig. 2.

From Eq. (21), the orbital period $T_t$ of the non-Keplerian orbit is

$$T_t = \frac{2\,\pi}{\sqrt{\mu_\odot/r_0^3}}\,\exp\left(2\,\widetilde{r}_t\right) \tag{22}$$

A linear stability analysis reveals that this non-Keplerian orbit is unstable. In fact, from Eq. (4), the derivative of the radial acceleration component is

$$\frac{\partial \ddot{r}}{\partial r} = \frac{\mu_\odot}{r_0^2}\,\left[2\,\exp\left(-2\,\widetilde{r}\right) - 3\,\exp\left(-3\,\widetilde{r}\right) - \beta\left(r_0/r_\oplus\right)\,\exp\left(-\widetilde{r}\right)\right] \tag{23}$$

Therefore, when $\beta = \beta^\star$ and $\widetilde{r} = \widetilde{r}_t$, Eq. (23) states that $\partial\ddot{r}/\partial r \simeq 0.0349\,\mu_\odot/r_0^2 > 0$.

To summarize, in this case the spacecraft heliocentric trajectory presents a single perihelion point ($P_0$ in the energy plane) at a distance $r_0$ from the Sun, and the maximum attainable distance ($r_t$) depends linearly on $r_0$.

#### *3.1.2 Case b*

When the slope of the energy line is sufficiently high (that is, $\beta > \beta^\star$), $P_0$ is the only intersection point between the energy line and the potential well boundary, see Fig. 1. In this case, for all $t > t_0$, the spacecraft is pushed away from the Sun and eventually reaches the escape condition $\widetilde{\mathcal{E}} = 0$ at a distance [see Eqs. (13) and (14)]:

$$r_e = r_0\,\exp\left(\frac{r_\oplus}{2\,\beta\,r_0}\right) \tag{24}$$

If the mission requirement is to reach a given hyperbolic excess velocity $V_\infty$ with respect to the Sun, the E-sail can be jettisoned when the Sun-spacecraft distance is:

$$r = r_0\,\exp\left(\frac{r_\oplus\,V_\infty^2 + \mu_\odot\,r_\oplus/r_0}{2\,\mu_\odot\,\beta}\right) \tag{25}$$

In this case, $P_0$ is the only trajectory point in which the radial velocity component is zero and $r_0$ is the corresponding perihelion distance. Figure 3 shows the spacecraft heliocentric trajectory when $\beta = 1.1\,\beta^\star \simeq 0.223995\,r_\oplus/r_0$. Note that, according to Eq. (24), the escape condition occurs at a distance $r_e \simeq 9.3\,r_0$ from the Sun.

#### *3.1.3 Case c*

The last case is obtained when the energy line intercepts the potential well boundary at three points, $P_0$, $P_a = (\widetilde{r}_a,\, \widetilde{\mathcal{E}}_a)$ and $P_b = (\widetilde{r}_b,\, \widetilde{\mathcal{E}}_b)$, as is shown in Fig. 1. This situation is representative of a low-performance propulsion system, that is, an E-sail with a low characteristic acceleration ($\beta < \beta^\star$). The values of $\widetilde{r}_a$ and $\widetilde{r}_b$, with $0 < r_a < r_t < r_b$, are two of the three real solutions of the nonlinear equation $\widetilde{\mathcal{E}} = \widetilde{\mathcal{E}}_w$, where $\widetilde{\mathcal{E}}$ is given by Eq. (14) and $\widetilde{\mathcal{E}}_w$ by Eq. (15). The nonlinear equation $\widetilde{\mathcal{E}} = \widetilde{\mathcal{E}}_w$ in the unknown $\widetilde{r}$ can be solved numerically, and the solution $\widetilde{r} = 0$ can be discarded as it coincides with $r_0$. The least of the remaining two solutions corresponds to $\widetilde{r}_a$, that is, the aphelion distance. To simplify the succeeding spacecraft trajectory analysis, Fig. 4 shows the values of aphelion distance $r_a/r_0$ as a function of the dimensionless characteristic acceleration $\beta < \beta^\star$. The same figure also shows the spacecraft radial acceleration component, which can be obtained from Eq. (4) when $r = r_a$.

Figure 4(b) shows that $\ddot{r}_a < 0$ for $\beta \in (0,\, \beta^\star)$, whereas $\ddot{r}_a = 0$ when $\beta = \{0,\, \beta^\star\}$. The special case of $\beta = 0$ is of scarce importance, as it corresponds to a spacecraft without any propulsion system. In that case the spacecraft tracks the initial circular parking orbit and the energy line reduces to the point $P_0$.

The spacecraft motion can be described as follows. Assuming that $\beta \in (0,\, \beta^\star)$, for $t > t_0$ the spacecraft increases its distance from the Sun until, at time $t_a$, it reaches a distance $r_a < r_t$ (point $P_a$ of Fig. 1). During this phase the spacecraft tracks, in the energy plane, the segment $\overline{P_0 P_a}$. Because $P_a$ belongs to the potential well boundary, at $P_a$ the spacecraft radial velocity component is zero, but the radial acceleration component is negative (see Fig. 4(b)). Therefore the spacecraft is subjected to a net inward force, proportional to $\ddot{r}_a$, that curves the trajectory toward the Sun. As a result the distance from the Sun starts decreasing and the spacecraft tracks backwards the segment $\overline{P_0 P_a}$ until it reaches $P_0$ again (at time $t_1$). Note that the spacecraft polar angle $\theta_1 \triangleq \theta(t_1)$ is, in general, different from $\theta_0 + 2\,k\,\pi$, where $k$ is a positive integer. For $t > t_1$ the motion in the energy plane repeats, that is, the spacecraft increases its distance from the Sun until $r_a$ and so on. In other words the spacecraft oscillates indefinitely, in the energy plane, along the segment $\overline{P_0 P_a}$. Clearly, the point $P_b$ cannot be reached because the segment $\overline{P_a P_b}$ lies in the forbidden region. Therefore, the value of $\beta^\star$, given by Eq. (20), is the minimum dimensionless characteristic acceleration required to escape from the circular parking orbit of radius $r_0$. In addition, $r_t$ is the maximum aphelion distance of a closed orbit when the propulsion system is on. When viewed with respect to a heliocentric reference frame, the spacecraft trajectory is constrained within the region between the two circles of radius $r_0$ (perihelion) and $r_a$ (aphelion). For example Fig. 5 illustrates the spacecraft trajectory for $\beta = 0.9\,\beta^\star \simeq 0.183269\, r_\oplus / r_0$, in which the aphelion distance is $r_a \simeq 2.06\, r_0$, a value which is in agreement with Fig. 4(a).

### *3.2 Elliptic Parking Orbit*

If the parking orbit is elliptic, that is, $e_0 \in [0, 1)$, both the potential well boundary and the energy line location depend on the starting polar angle $\theta_0$, see Eqs. (14)–(15). For a given value of $e_0$ the position of $P_0$ in the energy plane changes with $\theta_0$ as is shown in Fig. 6 for $e_0 = 0.3$. Note that when $\theta_0 \in \{0, 180\}$ deg the point $P_0$ belongs to the potential well boundary, whereas for $\theta_0 \in (0, 180)$ deg the point $P_0$ is inside the allowable region.

For a given quadruple $(p_0,\, e_0,\, \theta_0,\, \beta)$ the potential well boundary and the energy line are univocally defined, and the analysis of the spacecraft motion coincides with that described in the last section. In particular, the minimum value $\beta^\star$ of the dimensionless characteristic acceleration required to escape from the Sun is now a function of the triplet $(p_0,\, e_0,\, \theta_0)$. Bearing in mind Eqs.(14) and (15), the numerical solutions of Eqs. (17) have been summarized in Fig. 7 where, for symmetry reasons, the analysis of the initial polar angle range has been confined to $\theta_0 \in [0,\, 180]$ deg.

A few remarks are in order. For a circular parking orbit, both $\beta^\star$ and $\widetilde{r}_t$ are constant with respect to the starting polar angle $\theta_0$, and their values are in agreement with Eq. (20). More important, Fig. 7(a) shows that, for a given value of the pair $(p_0, e_0)$, the parameter $\beta^\star$ increases with $\theta_0$. Therefore, for a given parking orbit, the minimum value of the dimensionless characteristic acceleration $\beta^\star_{\text{min}} \triangleq \min[\beta^\star(\theta_0)]$ is obtained when $\theta_0 = 0$, that is, when the propulsion system is switched-on at the initial perihelion [12]. Figure 8 shows the required value of $\beta^\star_{\text{min}}$ as a function of $p_0$ and $e_0$.

The quantity $\beta^\star_{\text{min}}\, p_0/r_\oplus$ is almost linear with $e_0$, and can be approximated (with errors less than 0.6%) by the function

$$\beta^\star_{\text{min}} \frac{p_0}{r_\oplus} \simeq -0.2036\, e_0 + 0.2036 \tag{26}$$

Figure 8 and Eq. (26) reveal that $\beta^\star_{\text{min}} \to 0$ as $e_0 \to 1$. However this corresponds to the special case of a parabolic parking orbit and, indeed, the spacecraft reaches the escape condition at $t = 0$ without the need of any propulsion system.

As an example, if the elliptic parking orbit coincides with the Earth's heliocentric orbit of semimajor axis $a_0 = 1\,\text{AU}$ and eccentricity $e_0 = 0.0167102$, one obtains that $\beta^\star_{\text{min}} \simeq 0.201$ (the characteristic acceleration is $1.19\,\text{mm/s}^2$). Starting instead from the Mercury's heliocentric orbit ($a_0 = 0.3870989\,\text{AU}$ and $e_0 = 0.2056307$) the value of $\beta^\star_{\text{min}}$ increases to about 0.449 and the minimum characteristic acceleration required to escape is $2.662\,\text{mm/s}^2$.

## 4 Attainment of a Given Distance from the Sun

As a second practical application of the potential well's concept consider now the problem of finding the minimum characteristic acceleration required to reach a prescribed distance $R$ from the Sun. Without any loss of generality, a circular parking orbit of radius $r_0$ is assumed. Indeed, the extension to an elliptic parking orbit is straightforward. Unlike the previous analysis, in this case the propulsion system can be switched-off one time along the trajectory to model a situation in which the E-sail is jettisoned. To solve the problem, it is useful to distinguish between the following three cases.

#### *4.0.1 Case a*

Assume first that $\widetilde{R} \in (0, \widetilde{r}_t]$, where $\widetilde{r}_t$ is given by Eq. (20). In the energy plane the parking orbit is defined by the point $P_0 = (0, -1/2)$ while the target point belongs to a vertical line of equation $\widetilde{r} = \widetilde{R}$. The dimensionless specific mechanical energy at the intersection point $P_R = (\widetilde{R}, \widetilde{\mathcal{E}}_R)$ between this vertical line and the potential well boundary is obtained from Eq. (15):

$$\widetilde{\mathcal{E}}_R = \frac{1}{2}\,\exp(-2\,\widetilde{R}) - \exp(-\widetilde{R}) \tag{27}$$

with $\widetilde{\mathcal{E}}_R > -1/2$ for $\widetilde{R} > 0$. Because for $t > t_0$ the spacecraft tracks an energy line whose slope is proportional to the dimensionless characteristic acceleration [see Eq. (14)], the value of $\beta_{\min}$ is

$$\beta_{\min} = \frac{r_\oplus}{\widetilde{R}\,r_0}\left(\widetilde{\mathcal{E}}_R + 1/2\right) \equiv \frac{r_\oplus}{2\,\widetilde{R}\,r_0}\left[\exp(-2\,\widetilde{R}) - 2\,\exp(-\widetilde{R}) + 1\right] \tag{28}$$

In other terms, when $\beta = \beta_{\min}$ the spacecraft moves along the segment $\overline{P_0 P_R}$, and reaches the target distance $\widetilde{R}$ at the aphelion of the transfer trajectory, as is shown in Fig. 9.

For example, assume that $R = 1.524\,\mathrm{AU}$ (a value corresponding to the Sun-Mars mean distance), and a parking circular orbit of radius $r_0 \equiv r_\oplus$. In this case $\widetilde{R} \simeq 0.421338$ and, from

Eq. (28), $\beta_{\min} \simeq 0.140291$, that is, $a_{\oplus} \simeq 0.832\,\mathrm{mm/s^2}$. The spacecraft transfer trajectory is shown in Fig. 10.

#### *4.0.2 Case b*

If $\widetilde{R} > \widetilde{r}_t$, a portion of the segment $\overline{P_0 P_R}$ belongs to the forbidden region of the energy plane and the previous transfer strategy fails. In this case, as $P_R$ is on the right of $P_t$ (see Fig. 11), the optimal solution is simply the energy line that passes through $P_0$ and $P_t$. From Eq. (20), the minimum value of the dimensionless characteristic acceleration is:

$$\beta_{\min} > 0.203632 \left(\frac{r_{\oplus}}{r_0}\right) \tag{29}$$

Assuming $R = 5.2\,\mathrm{AU}$, equal to the Sun-Jupiter mean distance, and $r_0 \equiv r_{\oplus}$, the dimensionless distance is $\widetilde{R} \simeq 1.648658$ and the minimum characteristic acceleration is $a_{\oplus} \simeq 1.2087\,\mathrm{mm/s^2}$. The spacecraft transfer trajectory is shown in Fig. 12.

#### *4.0.3 Case c*

Finally, assume that the target distance is less than $r_0$, or $\widetilde{R} < 0$. In this case a transfer without an E-sail jettison is unfeasible, because the propulsion system provides an outward radial thrust only. However the target distance can be reached using a Keplerian orbit whose perihelion distance is $r_p \leq R$. Because the spacecraft can be transferred only towards Keplerian orbits whose semilatus rectum is $p_0 \equiv r_0$, the equation $r_p \leq R$ represents a constraint on the minimum aphelion radius $r_a$ of the candidate Keplerian orbit, that is:

$$r_a \geq \frac{r_0\, R}{2\, R - r_0} \tag{30}$$

In particular, Eq. (30) states that the spacecraft cannot reach a distance from the Sun less than $r_0/2$.

Assuming $R > r_0/2$ (that is, $\widetilde{R} > \log(1/2) \simeq -0.6931$), from a geometric viewpoint the optimal mission strategy corresponds to transfer the spacecraft to a Keplerian orbit whose perihelion radius $r_p$ is equal to $R$. For a given value of $r_p = R$, the corresponding Keplerian orbit is represented, in the energy plane, by a horizontal segment ranging from $P_p = (\widetilde{R}, \widetilde{\mathcal{E}}_R)$ to $P_a = (\widetilde{r}_a, \widetilde{\mathcal{E}}_R)$, see Fig. 13, where

$$\widetilde{r}_a \triangleq \log\left(\frac{R}{2\,R - r_0}\right) \tag{31}$$

and $\widetilde{\mathcal{E}}_R$ is given by Eq. (27). Note that $P_p$ and $P_a$ map, in the energy plane, the perihelion and the aphelion point of the Keplerian orbit, respectively.

The minimum value of the dimensionless characteristic acceleration required to reach a point of the segment $\overline{P_p P_a}$, depends on the horizontal position of $P_a$, that is, on the value of $\widetilde{r}_a$. In fact, for $\widetilde{r}_a \leq \widetilde{r}_t$, with $\widetilde{r}_t$ given by Eq. (21), the minimum value of $\beta$ corresponds to the transfer orbit that reaches the Keplerian orbit at its aphelion $P_a$, viz.

$$\beta_{\min} = \frac{r_\oplus}{\widetilde{r}_a\, r_0}\left(\widetilde{\mathcal{E}}_R + 1/2\right) \equiv \frac{r_\oplus}{2\,\widetilde{r}_a\, r_0}\left[\exp(-2\,\widetilde{R}) - 2\,\exp(-\widetilde{R}) + 1\right] \tag{32}$$

The E-sail is jettisoned exactly at a distance $r_a$ from the Sun, where $r_a$ is given by the right hand side of Eq. (30). This strategy is summarized in Fig. 13(a). For example, if $R = 0.723\,\mathrm{AU}$, equal to the Sun-Venus mean distance, and $r_0 \equiv r_\oplus$, the target distance is $\widetilde{R} \simeq -0.324346$ and $\widetilde{r}_a \simeq 0.483090 < \widetilde{r}_t$. From Eq. (32), the minimum dimensionless characteristic acceleration is $\beta_{\min} \simeq 0.1519$ (that is $a_\oplus \simeq 0.901\,\mathrm{mm/s^2}$), and the spacecraft transfer trajectory is shown in Fig. 14 along with the corresponding Keplerian orbit.

As was discussed in Case b, when $\widetilde{r}_a > \widetilde{r}_t$ the minimum dimensionless characteristic acceleration is equal to $\beta^\star$, see Eq. (29), and the E-sail is jettisoned at a distance $r_j < r_a$. This situation is illustrated in Fig. 13(b) and the jettison distance is

$$r_j = r_0 \, \exp\left(\frac{\widetilde{\mathcal{E}}_R + 1/2}{\beta^\star \, r_0/r_\oplus}\right) \equiv r_0 \, \exp\left(\frac{\exp(-2\,\widetilde{R}) - 2\,\exp(-\widetilde{R}) + 1}{2\,\beta^\star \, r_0/r_\oplus}\right) \tag{33}$$

For example, if $r_0 \equiv r_\oplus$ and $R = 0.55\,\mathrm{AU}$ ($\widetilde{R} \simeq -0.597837$), the E-sail jettison distance is $r_j \simeq 5.174\,\mathrm{AU}$ and the transfer trajectory is shown in Fig. 15.

## 5 Reaching a Keplerian Orbit of Given Period

The third practical application of the potential well's concept is the study of the minimum characteristic acceleration $\beta_{\min}$ required to reach a heliocentric Keplerian closed orbit of given period $T_k$. By assumption, the target Keplerian orbit is coplanar to the circular parking orbit of radius $r_0$. Moreover, the E-sail can be jettisoned at a suitable point of the transfer trajectory.

As discussed in the previous section, the target Keplerian orbit in the energy plane is represented by a horizontal segment whose dimensionless specific mechanical energy $\widetilde{\mathcal{E}}_k$ is

$$\widetilde{\mathcal{E}}_k \triangleq -\frac{r_0}{2\sqrt[3]{T_k^2\,\mu_\odot/(4\,\pi^2)}} \tag{34}$$

The segment endpoints, $P_p = (\widetilde{r}_p, \widetilde{\mathcal{E}}_k)$ and $P_a = (\widetilde{r}_a, \widetilde{\mathcal{E}}_k)$, map the target Keplerian orbit perihelion and aphelion points, respectively, where $\widetilde{r}_p = \log(r_p/r_0)$ and $\widetilde{r}_a = \log(r_a/r_0)$ with

$$r_p = \sqrt[3]{T_k^2\,\mu_\odot/(4\,\pi^2)}\left(1 - \sqrt{1 - \frac{r_0}{\sqrt[3]{T_k^2\,\mu_\odot/(4\,\pi^2)}}}\right) \tag{35}$$

$$r_a = \sqrt[3]{T_k^2\,\mu_\odot/(4\,\pi^2)}\left(1 + \sqrt{1 - \frac{r_0}{\sqrt[3]{T_k^2\,\mu_\odot/(4\,\pi^2)}}}\right) \tag{36}$$

In fact, because the semilatus rectum $p_k$ of the target Keplerian orbit is equal to $r_0$, the semimajor axis $a_k$ and the eccentricity $e_k$ of the final orbit are obtained as

$$a_k = \sqrt[3]{T_k^2\,\mu_\odot/(4\,\pi^2)} \tag{37}$$

$$e_k = \sqrt{1 - \frac{r_0}{a_k}} \equiv \sqrt{1 - \frac{r_0}{\sqrt[3]{T_k^2\,\mu_\odot/(4\,\pi^2)}}} \tag{38}$$

Note that the constraint $p_k = r_0$ implies that a transfer towards an orbit of period $T_k < T_0 \triangleq 2\,\pi\,\sqrt{r_0^3/\mu_\odot}$ (or $\widetilde{\mathcal{E}}_k < -1/2$) is infeasible. Therefore assume that $T_k > T_0$, as $T_k = T_0$ corresponds to a situation in which at time $t_0$ the spacecraft is already on the target Keplerian orbit. The problem can be solved in the energy plane with the aid of the two cases illustrated in Fig. 16.

#### 5.0.4 *Case a*

The dimensionless specific mechanical energy of the target Keplerian orbit ranges in the interval $\widetilde{\mathcal{E}}_k \in (-1/2, \widetilde{\mathcal{E}}_t]$, where $\widetilde{\mathcal{E}}_t \simeq -0.244150$ is the ordinate of point $P_t$. In this case $\widetilde{r}_a \leq \widetilde{r}_t$ and, as was discussed in the previous section, the optimal strategy is to reach the Keplerian orbit aphelion where the E-sail is jettisoned. The minimum required dimensionless characteristic acceleration is

$$\beta_{\min} = \frac{r_\oplus}{\widetilde{r}_a\,r_0}\left(\widetilde{\mathcal{E}}_k + 1/2\right) \tag{39}$$

and the jettison distance is $r_j = r_a$, see Eq. (36).

#### 5.0.5 *Case b*

The dimensionless specific mechanical energy of the target Keplerian orbit ranges in the interval $\widetilde{\mathcal{E}}_k \in (\widetilde{\mathcal{E}}_t, 0)$, that is, the dimensionless aphelion radius is greater than $\widetilde{r}_t$. In this case the optimal strategy requires that $\beta_{\min} = \beta^\star$ [see Eq. (20)], and the jettison distance $r_j$ is given by

$$r_j = r_0\,\exp\left(\frac{\widetilde{\mathcal{E}}_k + 1/2}{\beta^\star\,r_0/r_\oplus}\right) \tag{40}$$

The previous relationships are useful for a preliminary mission analysis whose aim is to reach a Keplerian orbit in mean motion orbital resonance with the parking one. The transfer trajectory characteristics and the E-sail required performances have been summarized in Table 1 for some values of resonance ratio $T_k/T_0$. The resonance ratio corresponds to the number of spacecraft revolutions for one revolution of the given celestial body around the Sun. Note that for a given value of $r_0$, both the dimensionless characteristic acceleration $\beta_{\min}$ and the jettison distance $r_j$ increase with the resonance ratio $T_k/T_0$. In fact, an increment of the period $T_k$ increases both $\widetilde{\mathcal{E}}_k$ and $r_a$.

## 6 Nodal Flyby Missions to NEAs

The last mission application is related to a nodal flyby mission [21,22] towards a Near Earth Asteroid (NEA) whose population, calculated at mid-January 2011, consists of 7600 bodies [1]. In such a mission scenario, a spacecraft that moves in the ecliptic plane, performs a sequence of close encounters with NEAs. To this end, the spacecraft is transferred to a Keplerian orbit in mean motion orbital resonance with the target asteroid's orbit. Accordingly, a flyby occurs in one of the two nodes of the asteroid's heliocentric orbit, that is, when the Sun-spacecraft distance is $r_{\Omega}$ (ascending node) or $r_{\mho}$ (descending node) with

$$r_{\Omega} = \frac{a_n\,(1-e_n^2)}{1+e_n\,\cos\omega_n} \qquad , \qquad r_{\mho} = \frac{a_n\,(1-e_n^2)}{1+e_n\,\cos(\pi-\omega_n)} \tag{41}$$

where $a_n$ is the semimajor axis, $e_n$ is the eccentricity, and $\omega_n$ is the argument of periapsis of the target asteroid's heliocentric orbit.

The analysis of the problem in the energy plane detects the optimal strategy and provides an estimate of the minimum characteristic acceleration required to perform the transfer phase of

[1] The catalog of NEAs orbital elements is available online at `http://newton.dm.unipi.it/neodys/` [retrieved 14 January 2011].

the mission. To reduce the problem complexity, the ephemeris constraint is neglected, and a circular parking orbit of radius $r_0 = r_\oplus$ is assumed. In other terms, the problem is now to find the minimum value $\beta_{\min}$ and the jettison distance $r_j$ required to transfer the spacecraft from a circular parking orbit of radius $r_\oplus$ to an elliptic heliocentric orbit of given resonance ratio $q \triangleq T_k/T_n$, where $T_n = 2\,\pi\,\sqrt{a_n^3/\mu_\odot}$ is the asteroid's orbital period. For a given pair $(q, T_n)$, the optimal dimensionless characteristic acceleration $\beta_{\min}$ and the corresponding jettison distance $r_j$ are obtained with the approach described in the previous section.

Note that the constraint on the semilatus rectum states that the transfer is infeasible if $q < T_0/T_n$. Moreover, for a given value of $q > T_0/T_n$, the flyby is impossible if $\{r_\Omega, r_\mho\} \cap [r_p,\, r_a] = \{0\}$, where $r_p$ and $r_a$, that is, the perihelion and aphelion distances of the Keplerian orbit, are given by Eqs. (35)-(36) with $T_k = q\,T_n$.

The number of unreachable asteroids decreases with the resonance ratio $q$, as is shown in Fig. 17. For example, when $q = 1$ about 824 asteroids (10.8% of the entire population) are not reachable, whereas when $q = 2$ the number of "forbidden" asteroids reduces to 33 (0.43% only of the entire population). The horizontal asymptote in Fig. 17 shows that a nodal flyby mission is impossible for a set of 16 NEAs. For these asteroids the value of both $r_\Omega$ and $r_\mho$ is less than $r_0/2 = 0.5\,\mathrm{AU}$.

Figure 18 shows the minimum dimensionless characteristic acceleration $\beta_{\min}$ and the jettison distance $r_j$ as a function of the resonance ratio $q$ for the asteroids population. Note that the cumulative percent in the abscissa of Fig. 18 refers to the actually reachable asteroids for a given value of $q$, see also Fig. 17.

Figure 18(a) shows that the required value of $\beta_{\min}$ increases with $q$ and for $q > 3$ nearly all of the asteroids population is reachable with an E-sail of $\beta_{\min} = \beta^\star$. The resonance ratio $q$ is therefore an important parameter for assessing the E-sail capabilities in this mission type. In fact, when $a_\oplus \le 0.5\,\mathrm{mm/s^2}$ (or $\beta \le 0.0843$) the number of reachable asteroids is strongly dependent on the value of $q$, as is shown in Tab. 2.

## 7 Conclusions

A new graphical approach for the preliminary mission analysis of an E-sail spacecraft has been illustrated. Assuming the thrust is always oriented radial with respect to the Sun-spacecraft direction, the space vehicle is subjected to a propulsive, outward, acceleration that varies inversely proportional with the distance from the Sun. The assumption of radial thrust not only is a means to reduce the problem mathematical complexity, but could also be a potentially useful concept from an engineering viewpoint. Indeed, while in principle the E-sail can be slightly inclined and thereby produce an off-radial thrust, maintaining the sail nominal plane orthogonal to the solar wind flow during the whole mission would simplify the design of some spacecraft elements as, for example, thermal and high voltage subsystems. Therefore, it cannot be excluded that a purely radial thrust could be, in practice, an optimal engineering solution, or that if the E-sail nominal plane is inclined, a useful starting point for mission analysis could be provided by the purely radial propulsive acceleration approximation. In this scenario, the spacecraft trajectory is conveniently described in the energy plane, in which the feasible motion is constrained by the potential well concept. With a suitable choice of the independent variables, a new definition of energy plane and potential well has been introduced to obtain a problem solution through a graphical approach. In particular, the main orbital parameters, as the maximum and minimum attainable distance from the Sun, can be calculated by simply intersecting the potential well boundary with a straight line whose slope is proportional to the E-sail characteristic acceleration. As a result, a number of interesting problems involving an E-sail subject to a purely radial thrust can be solved using a semi-analytical approach, without the need to resort to lengthy numerical simulations.

## Acknowledgments

This research was financed in part within the European Community's Seventh Framework Programme ([FP7/2007-2013]) under grant agreement number 262733.

## References

[1] J. A. Kechichian, Optimal low-thrust transfer using variable bounded thrust, Acta Astronautica 36 (7) (1995) 357–365, doi: 10.1016/0094-5765(95)00112-3.

[2] G. Mengali, A. A. Quarta, Fuel-optimal, power-limited rendezvous with variable thruster efficiency, Journal of Guidance, Control, and Dynamics 28 (6) (2005) 1194–1199, doi: 10.2514/1.12480.

[3] M. Otten, C. R. McInnes, Near minimum-time trajectories for solar sails, Journal of Guidance, Control, and Dynamics 24 (3) (2001) 632–634, doi: 10.2514/2.4758.

[4] G. Mengali, A. A. Quarta, Optimal control laws for axially symmetric solar sails, Journal of Spacecraft and Rockets 42 (6) (2005) 1130–1133, doi: 10.2514/1.17102.

[5] P. Janhunen, The electrical sail - a new propulsion method which may enable fast missions to the outer solar system, Journal of the British Interplanetary Society 61 (2008) 322–325 .

[6] G. Mengali, A. A. Quarta, Non-keplerian orbits for electric sails, Celestial Mechanics and Dynamical Astronomy 105 (1–3) (2009) 179–195, doi: 10.1007/s10569-009-9200-y.

[7] G. Mengali, A. A. Quarta, P. Janhunen, Electric sail performance analysis, Journal of Spacecraft and Rockets 45 (1) (2008) 122–129, doi: 10.2514/1.31769.

[8] G. Mengali, A. A. Quarta, P. Janhunen, Considerations of electric sailcraft trajectory design, Journal of the British Interplanetary Society 61 (2008) 326–329 .

[9] A. A. Quarta, G. Mengali, P. Janhunen, Optimal interplanetary rendezvous combining electric sail and high thrust propulsion system, Acta Astronautica 68 (5-6) (2011) 603–621, doi: 10.1016/j.actaastro.2010.01.024.

[10] A. A. Quarta, G. Mengali, Electric sail missions to potentially hazardous asteroids, Acta Astronautica 66 (9-10) (2010) 1506–1519, doi: 10.1016/j.actaastro.2009.11.021.

[11] H. S. Tsien, Take-off from satellite orbit, Journal of the American Rocket Society 23 (4) (1953) 233–236 .

[12] G. Mengali, A. A. Quarta, Escape from elliptic orbit using constant radial thrust, Journal of Guidance, Control, and Dynamics 32 (3) (2009) 1018–1022, doi: 10.2514/1.43382.

[13] J. E. Prussing, V. L. Coverstone, Constant radial thrust acceleration redux, Journal of Guidance, Control, and Dynamics 21 (3) (1998) 516–518, doi: 10.2514/2.7609.

[14] P. Janhunen, Electric sail for spacecraft propulsion, Journal of Propulsion and Power 20 (4) (2004) 763–764, doi: 10.2514/1.8580.

[15] P. Janhunen, A. Sandroos, Simulation study of solar wind push on a charged wire: Basis of solar wind electric sail propulsion, Annales Geophysicae 25 (3) (2007) 755–767, doi: 10.5194/angeo-25-755-2007.

[16] P. Janhunen, The electric solar wind sail status report, in: European Planetary Science Congress 2010, Vol. 5, Rome, Italy, 2010, paper EPSC 2010-297.

[17] C. R. McInnes, Solar Sailing: Technology, Dynamics and Mission Applications, Springer-Praxis Series in Space Science and Technology, Springer-Verlag, Berlin, 1999, pp. 46–54, ISBN: 3-540-21062-8.

[18] J. L. Wright, Space Sailing, Gordon and Breach Science Publisher, Berlin, 1992, pp. 223–226, ISBN: 2-881-24842-X.

[19] R. H. Battin, An Introduction to the Mathematics and Methods of Astrodynamics, revised Edition, AIAA Education Series, AIAA, New York, 1999, pp. 408–415, ISBN: 1-563-47342-9.

[20] R. J. McKay, M. Macdonald, J. Biggs, C. R. McInnes, Survey of highly non-keplerian orbits with low-thrust propulsion, Journal of Guidance, Control and Dynamics 34 (3) (2011) 645–666, doi: 10.2514/1.52133.

[21] E. Perozzi, L. Casalino, G. Colasurdo, A. Rossi, G. B. Valsecchi, Resonant fly-by missions to near earth asteroids, Celestial Mechanics and Dynamical Astronomy 83 (1–4) (2002) 49–62, doi: 10.1023/A:1020122511548.

[22] R. P. Binzel, E. Perozzi, A. S. Rivkin, A. Rossi, A. W. Harris, S. J. Bus, G. B. Valsecchi, S. M. Slivan, Dynamical and compositional assessment of near-earth object mission targets, Meteoritics and Planetary Science 39 (3) (2004) 351–366, doi: 10.1111/j.1945-5100.2004.tb00098.x.

**List of Tables**

| $T_k/T_0$ | $r_p/r_0$ | $r_a/r_0$ | $\beta_{\min}\, r_0/r_\oplus$ | $r_j/r_0$ | Case |
|---|---|---|---|---|---|
| 2 | 0.6218 | 2.5530 | 0.1974 | 2.5530 | a |
| 3 | 0.5812 | 3.5790 | 0.2036 | 3.5786 | b |
| 4 | 0.5629 | 4.4768 | 0.2036 | 4.3972 | b |
| 5 | 0.5521 | 5.2959 | 0.2036 | 5.0313 | b |
| 6 | 0.5450 | 6.0589 | 0.2036 | 5.5388 | b |
| 7 | 0.5398 | 6.7788 | 0.2036 | 5.9560 | b |
| 8 | 0.5359 | 7.4641 | 0.2036 | 6.3063 | b |
| 9 | 0.5328 | 8.1207 | 0.2036 | 6.6056 | b |
| 10 | 0.5303 | 8.7529 | 0.2036 | 6.8648 | b |
| 3:2 | 0.6726 | 1.9481 | 0.1776 | 1.9481 | a |
| 5:2 | 0.5966 | 3.0874 | 0.2027 | 3.0874 | a |
| 7:2 | 0.5706 | 4.0398 | 0.2036 | 4.0159 | b |
| 9:2 | 0.5569 | 4.8945 | 0.2036 | 4.7330 | b |
| 4:3 | 0.7053 | 1.7175 | 0.1613 | 1.7175 | a |
| 5:3 | 0.6505 | 2.1609 | 0.1873 | 2.1609 | a |
| 7:3 | 0.6035 | 2.9149 | 0.2017 | 2.9149 | a |
| 10:3 | 0.5738 | 3.8891 | 0.2036 | 3.8769 | b |

Table 1
Optimal performance to obtain a mean motion orbital resonance with the parking orbit.

| | $q = 1$ | $q = 3{:}2$ | $q = 2$ |
|---|---|---|---|
| $a_\oplus \leq 0.07\,\mathrm{mm/s^2}$ | 1 | 0 | 0 |
| $a_\oplus \leq 0.2\,\mathrm{mm/s^2}$ | 5 | 2 | 0 |
| $a_\oplus \leq 0.1\,\mathrm{mm/s^2}$ | 2 | 0 | 0 |
| $a_\oplus \leq 0.3\,\mathrm{mm/s^2}$ | 19 | 7 | 1 |
| $a_\oplus \leq 0.4\,\mathrm{mm/s^2}$ | 45 | 15 | 2 |
| $a_\oplus \leq 0.5\,\mathrm{mm/s^2}$ | 88 | 25 | 3 |

Table 2
Number of reachable NEAs as a function of $a_\oplus$ and $q$.

## List of Figures

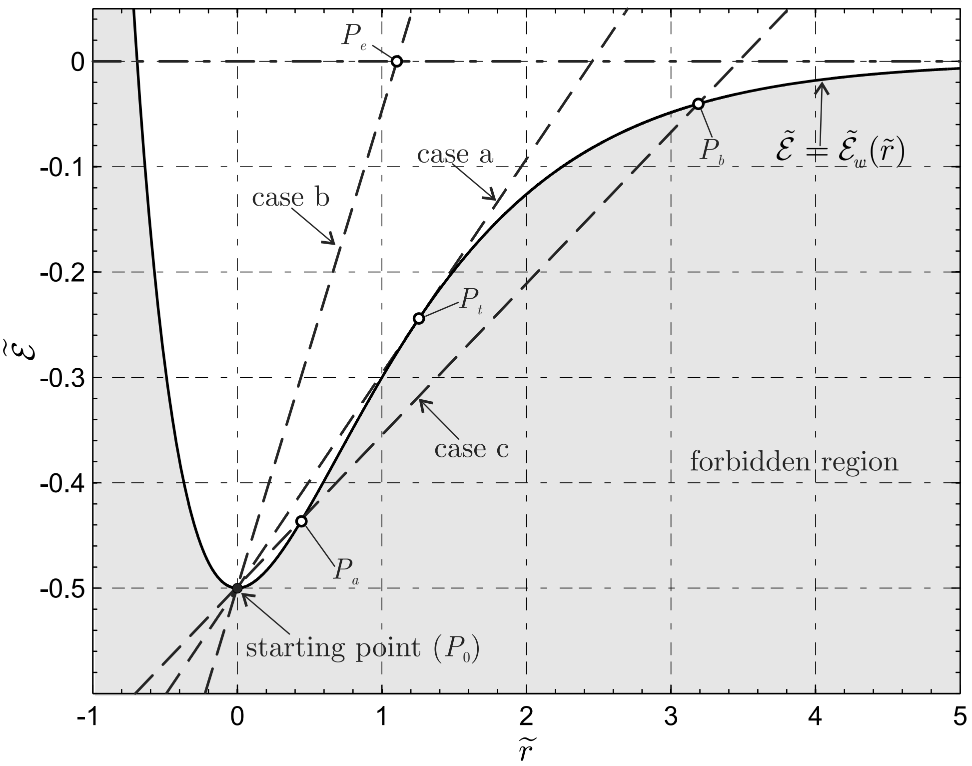


Figure 1. Potential well boundary for a circular parking orbit.

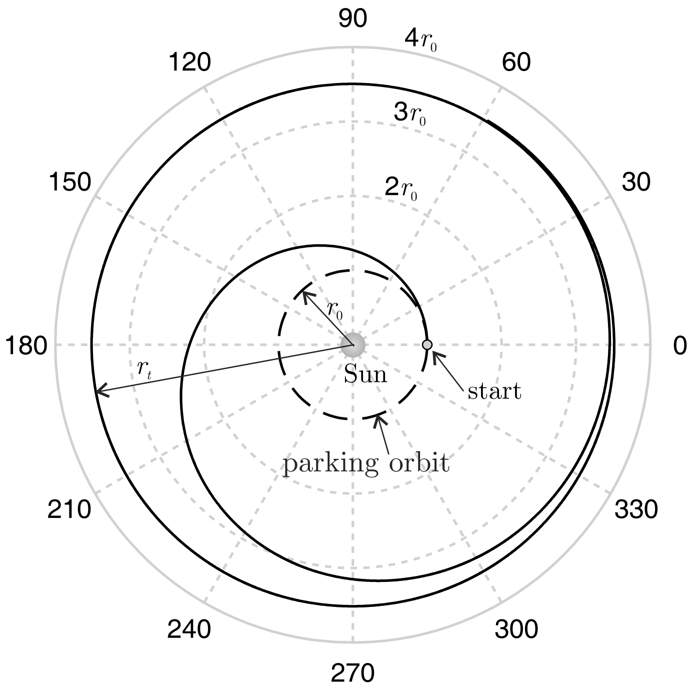


Figure 2. Spacecraft trajectory for $\beta = \beta^{\star}$, starting from a circular parking orbit of radius $r_0$

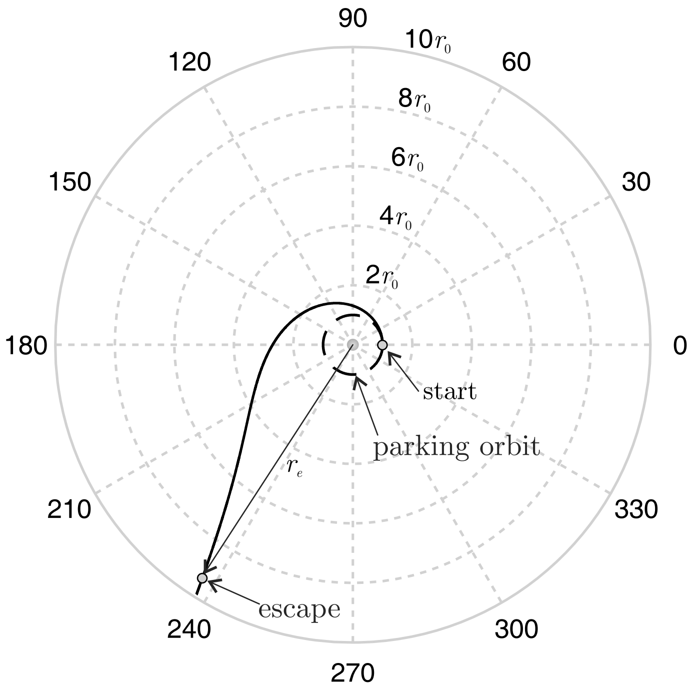


Figure 3. Spacecraft trajectory for $\beta = 1.1\,\beta^{\star} \simeq 0.223995\,r_{\oplus}/r_0$, starting from a circular parking orbit of radius $r_0$.

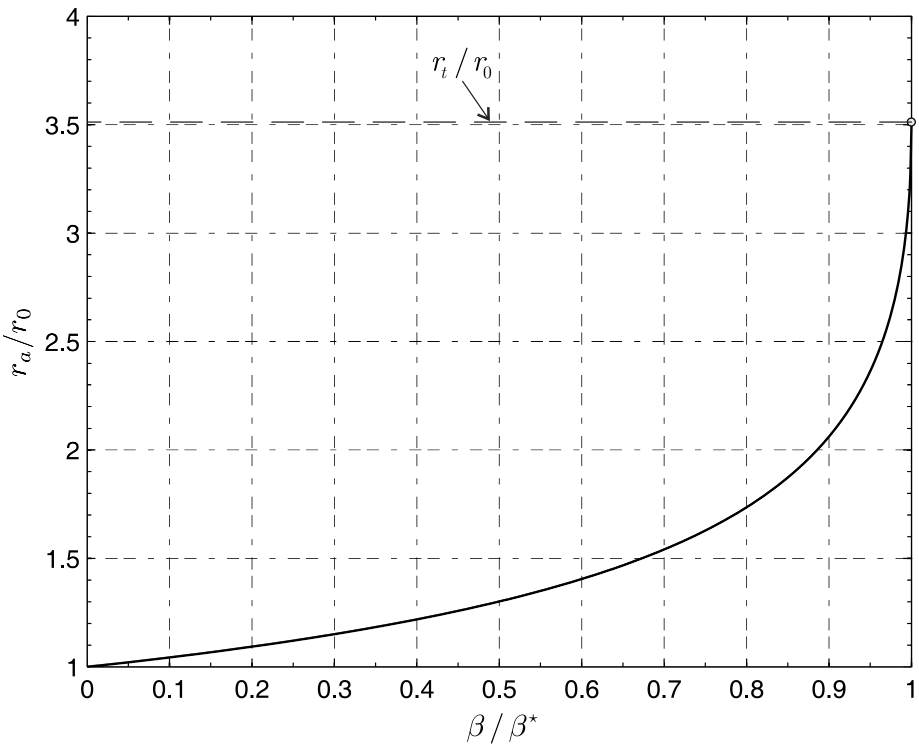


(a) Aphelion distance.

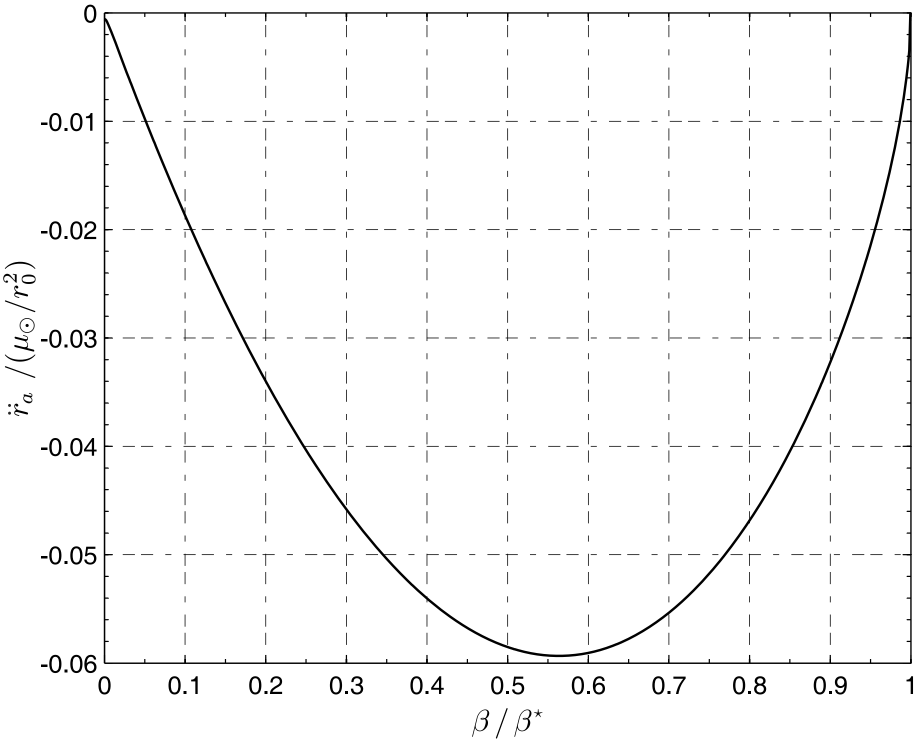


(b) Radial component of acceleration.

Figure 4. Aphelion distance and radial component of acceleration as a function of the dimensionless characteristic acceleration for a circular parking orbit of radius $r_0$.

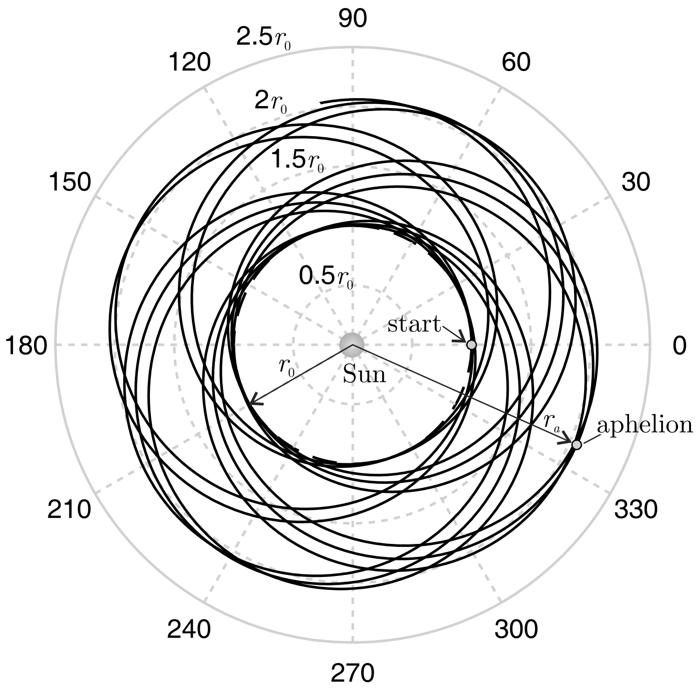


Figure 5. Spacecraft trajectory for $\beta = 0.9\,\beta^{\star} \simeq 0.183268\,r_{\oplus}/r_0$, starting from a circular parking orbit of radius $r_0$.

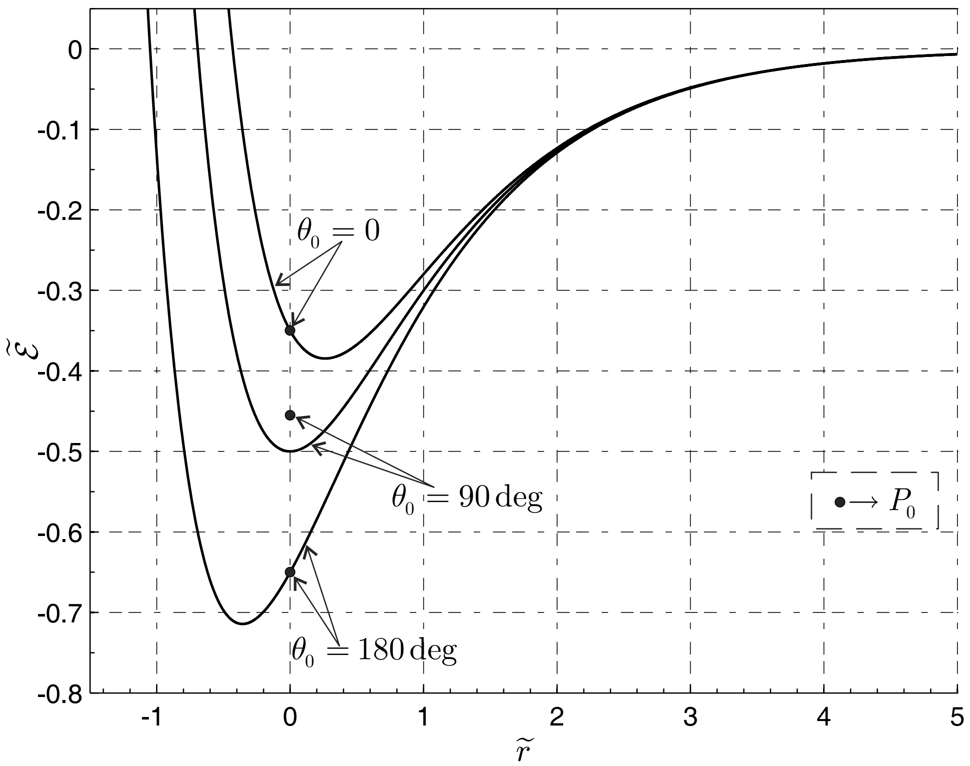


Figure 6. Potential well boundary and starting point $P_0$, for three values of the polar angle $\theta_0$, starting from an elliptic orbit of eccentricity $e_0 = 0.3$.

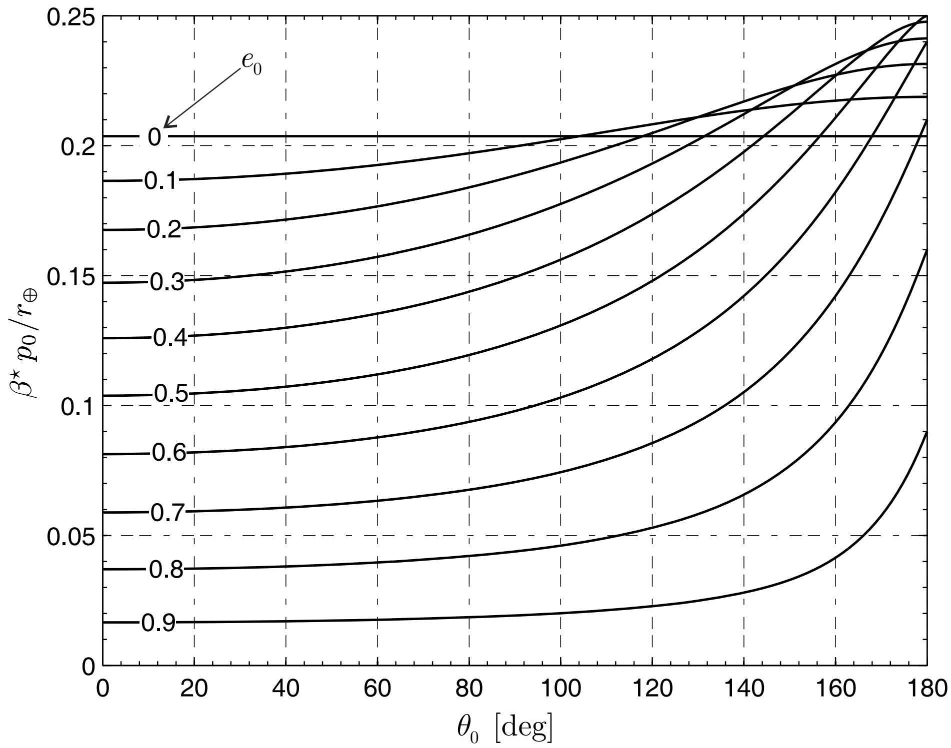


(a) Dimensionless characteristic acceleration $\beta^\star$.

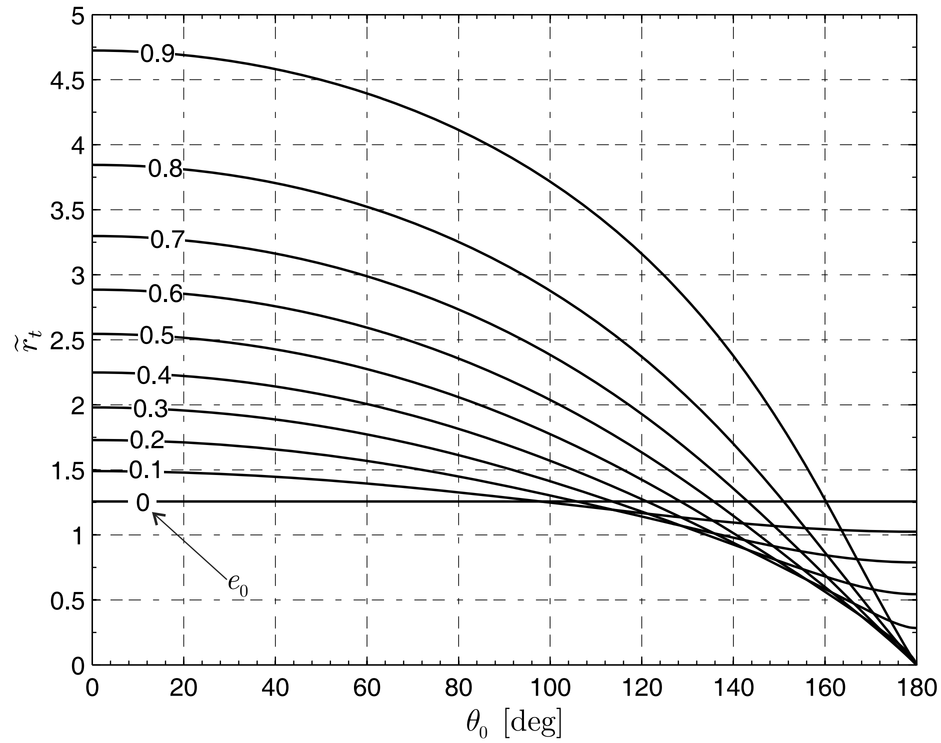


(b) Non-Keplerian orbit dimensionless radius $\widetilde{r}_t$.

Figure 7. Optimal performance for an escape mission as a function of the parking orbit characteristics $(p_0, e_0)$ and the initial polar angle $\theta_0$.

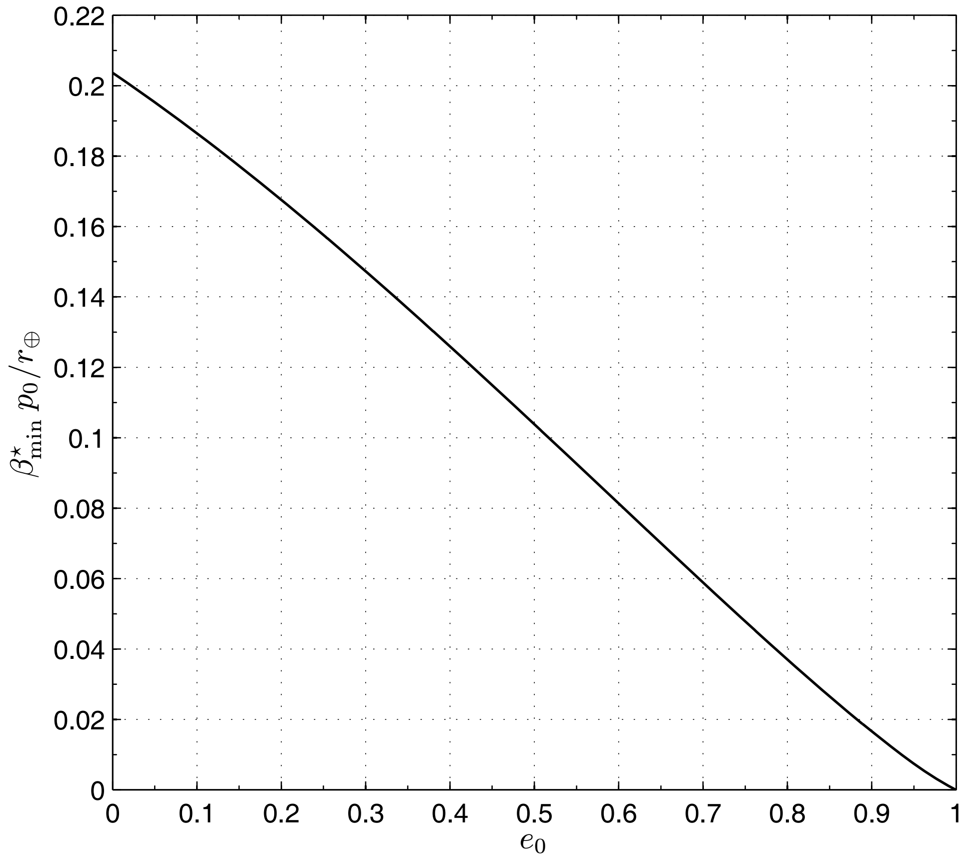


Figure 8. Minimum dimensionless characteristic acceleration $\beta^\star_{\min}$ required to escape from the Sun, as a function of the parking orbit characteristics $p_0$ and $e_0$.

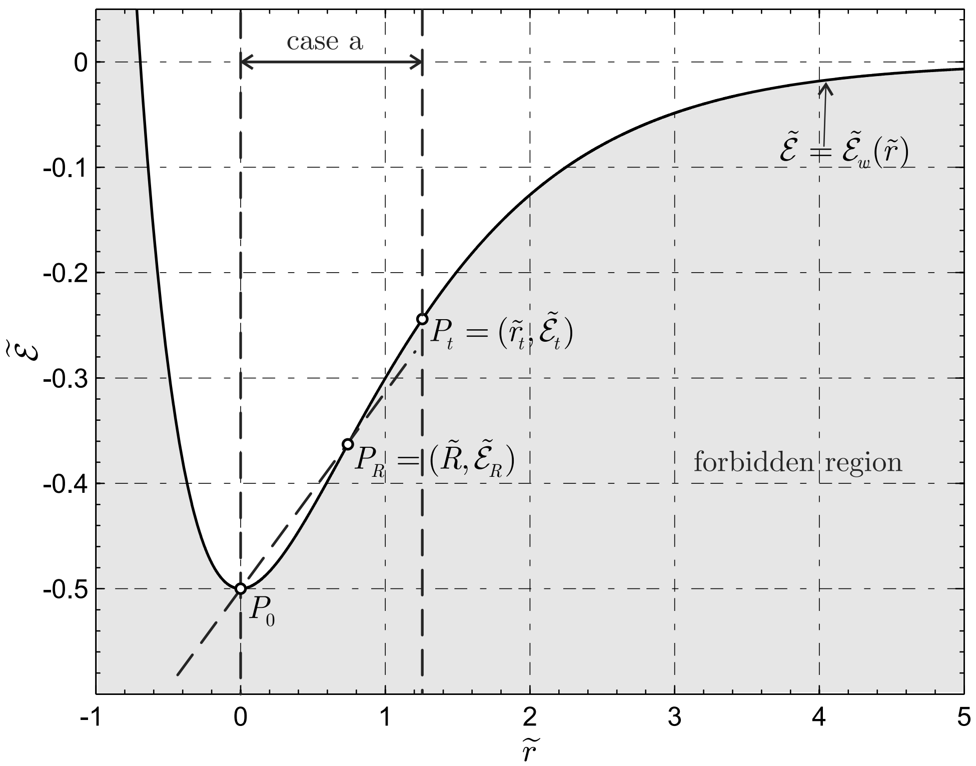


Figure 9. Optimal strategy to reach a (dimensionless) distance $\widetilde{R} \in (0, \widetilde{r}_t]$, starting from a circular parking orbit.

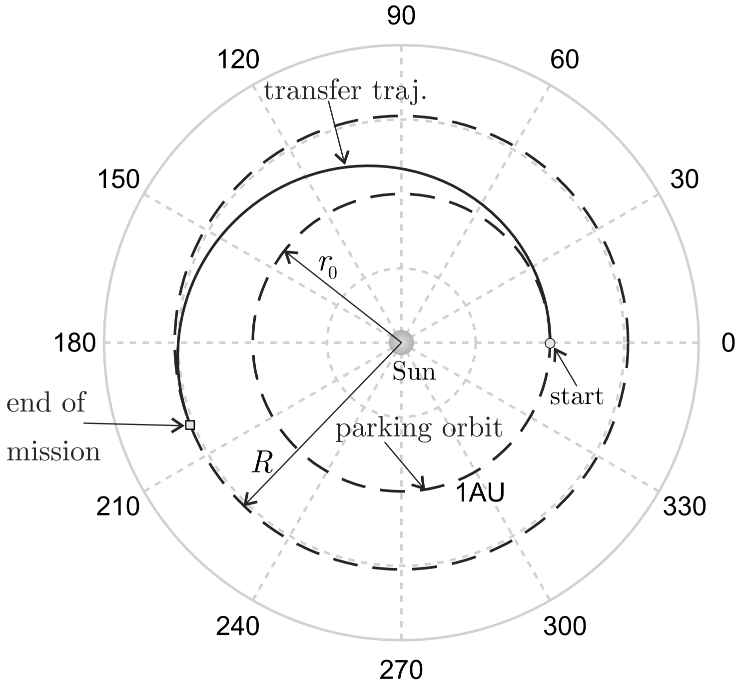


Figure 10. Optimal transfer trajectory to reach a distance $R = 1.524\,\mathrm{AU}$, starting from a circular parking orbit of radius $r_0 = r_\oplus$.

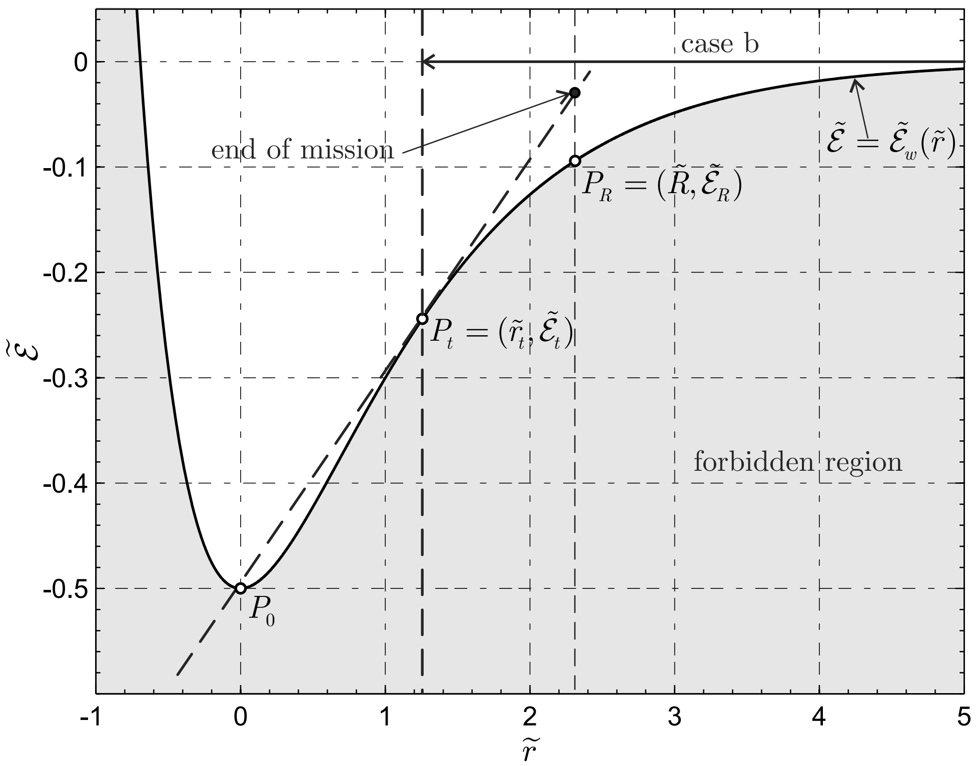


Figure 11. Optimal strategy to reach a (dimensionless) distance $\widetilde{R} > \widetilde{r}_t$, starting from a circular parking orbit.

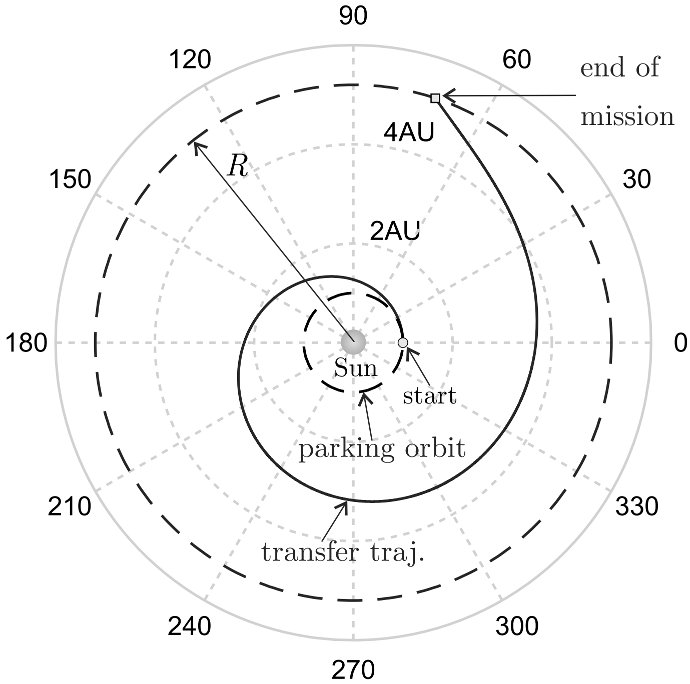


Figure 12. Optimal transfer trajectory to reach a distance $R = 5.2\,\mathrm{AU}$, starting from a circular parking orbit of radius $r_0 = r_\oplus$.

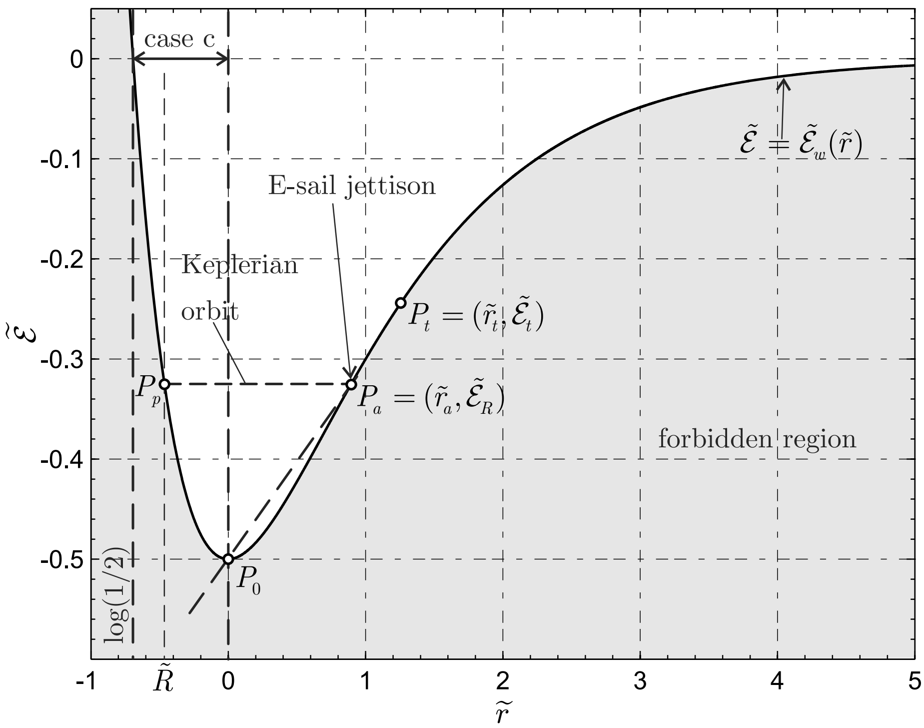


(a) $\widetilde{r}_a < \widetilde{r}_t$

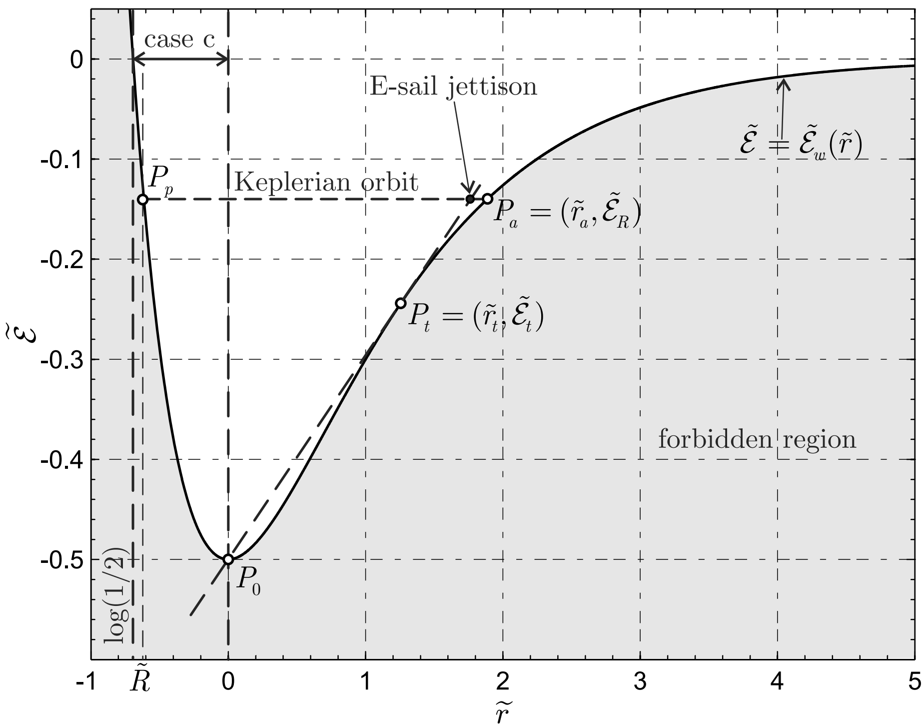


(b) $\widetilde{r}_a > \widetilde{r}_t$

Figure 13. Optimal strategy to reach a (dimensionless) distance $\widetilde{R} \in (\log(1/2), 0)$ as a function of $\widetilde{r}_a$, starting from a circular parking orbit.

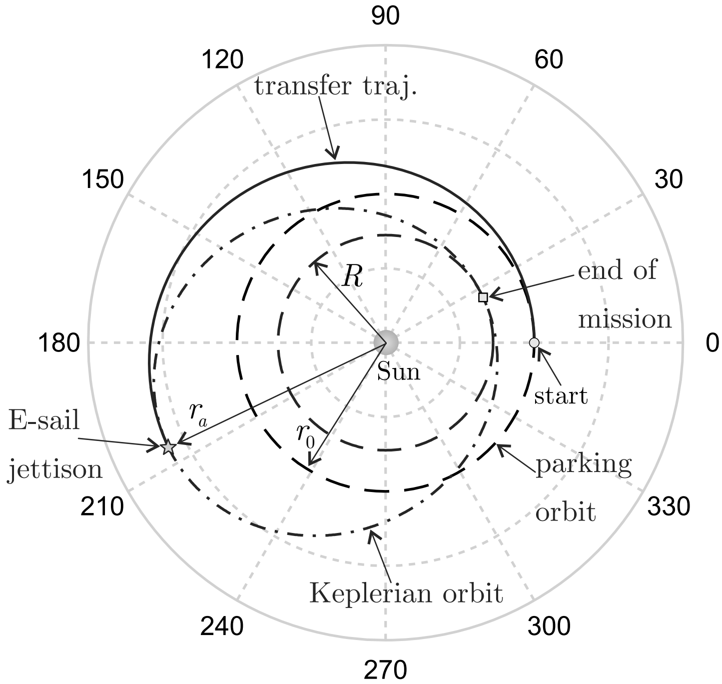


Figure 14. Optimal transfer trajectory to reach a distance $R = 0.723\,\mathrm{AU}$, starting from a circular parking orbit of radius $r_0 = r_\oplus$.

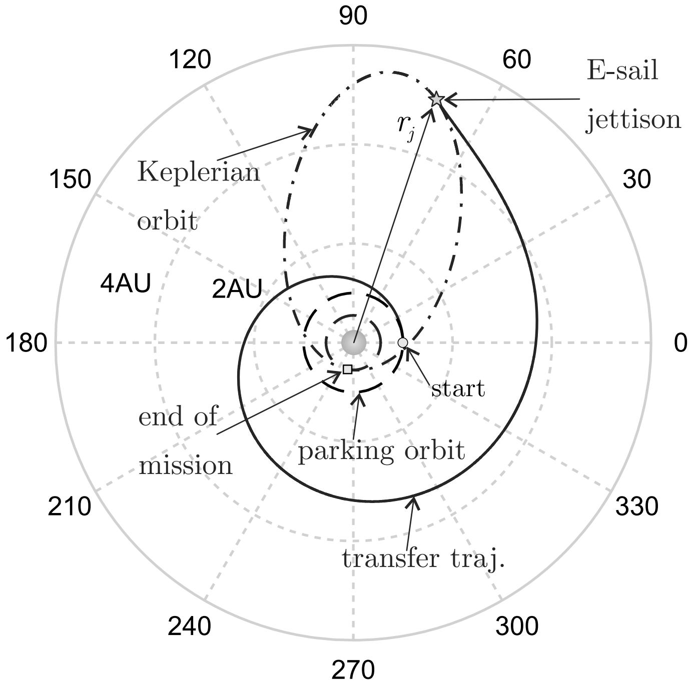


Figure 15. Optimal transfer trajectory to reach a distance $R = 0.55\,\mathrm{AU}$, starting from a circular parking orbit of radius $r_0 = r_\oplus$.

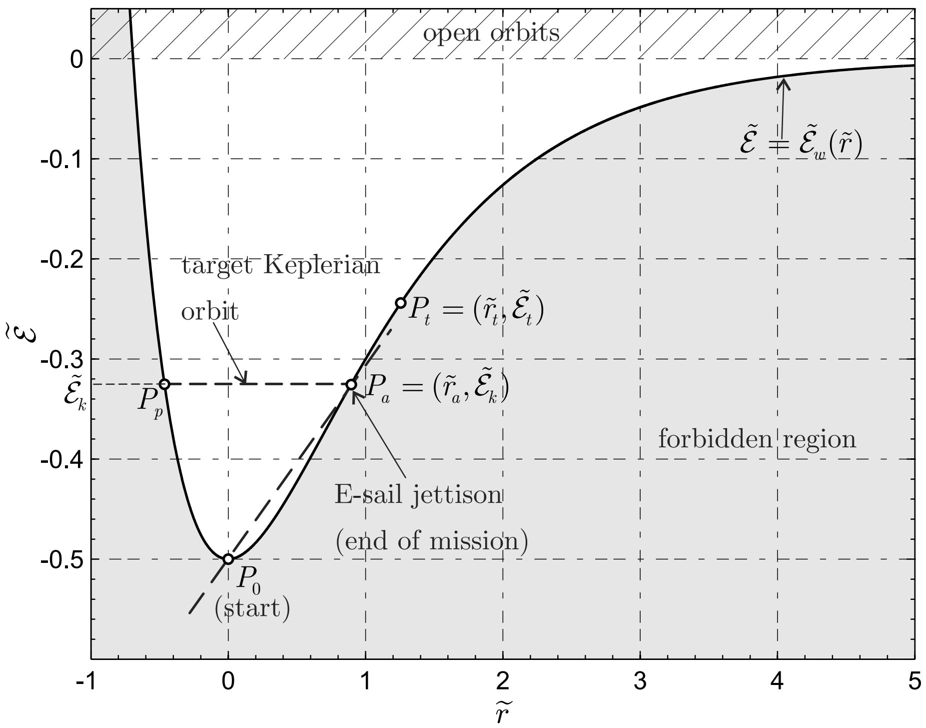


(a) Case a.

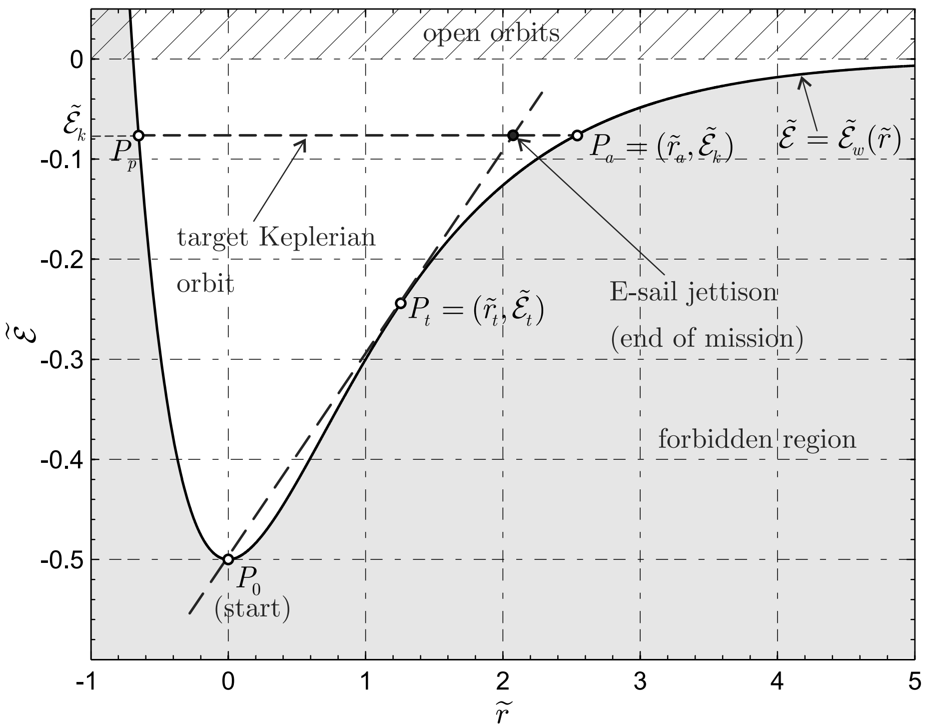


(b) Case b.

Figure 16. Optimal strategy to reach a heliocentric (closed) Keplerian orbit of given period, starting from a circular parking orbit.

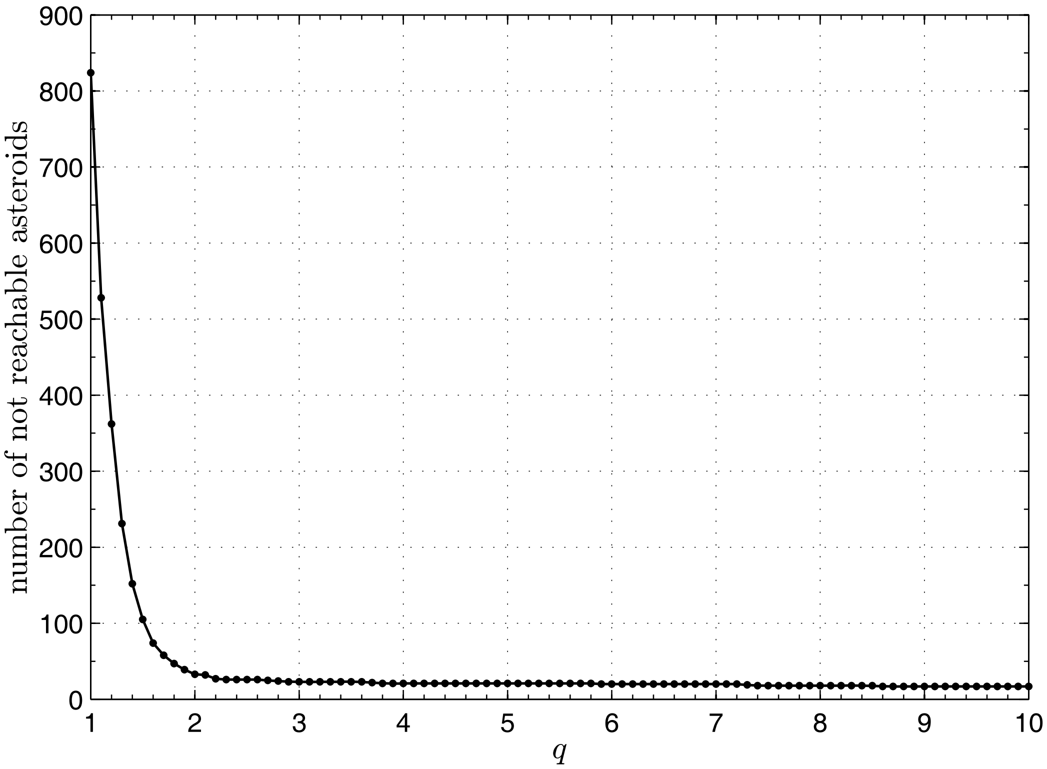


Figure 17. Number of unreachable asteroids as a function of the resonance ratio $q \geq 1$.

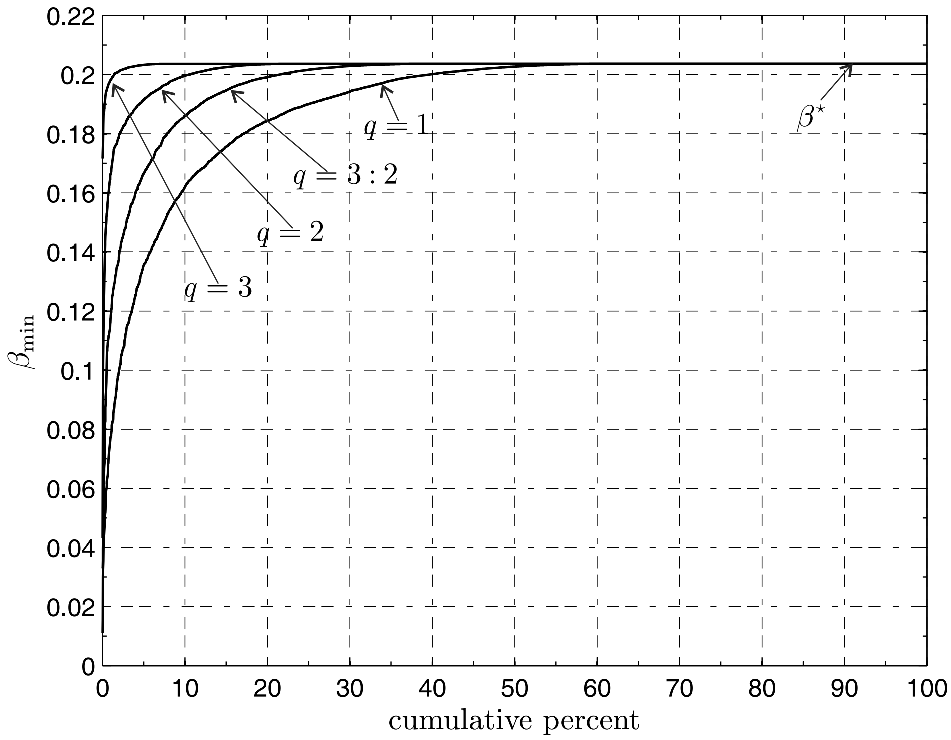


(a) Dimensionless characteristic acceleration.

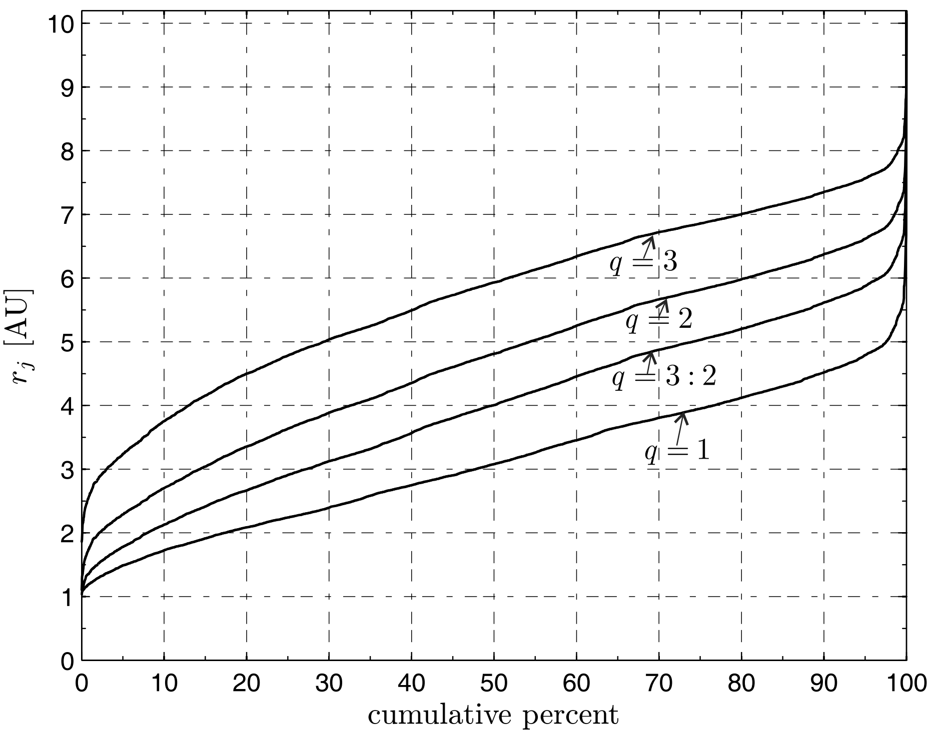


(b) Jettison distance.

Figure 18. Optimal performances for a nodal flyby mission towards a NEA, starting from a circular parking orbit of radius $r_0 = r_\oplus$.